Palmitoylated small GTPase ARL15 is translocated within Golgi network during adipogenesis

Yixing Wu[1$], Ying Bai[1$], David G. McEwan[2,3], Liz Bentley[1], Dimitra Aravani[1*], Roger D. Cox[1*]

1. Mammalian Genetics Unit, MRC Harwell Institute, Harwell Oxford, Oxfordshire, OX11 0RD, UK
2. Division of Cell Signalling & Immunology, School of Life Sciences, University of Dundee, Dundee, UK.
3. Cancer Research UK Beatson Institute, Garscube Estate, Switchback Road, Glasgow, G61 1BD, UK.

[*]**Corresponding Authors:** d.aravani@har.mrc.ac.uk, r.cox@har.mrc.ac.uk

[$] Equal contribution

Summary statement:

ARL15 (GTPase ARF family) is associated with adipose traits. ARL15 is palmitoylated, localised to Golgi in preadipocytes and translocated to other Golgi compartments during differentiation. ARL15 interacts with ER-localised ARL6IP5.

Abstract

The small GTPase ARF family member *ARL15* gene locus is associated in population studies with increased risk of type 2 diabetes, lower adiponectin and higher fasting insulin levels. Previously, loss of ARL15 was shown to reduce insulin secretion in a human β-cell line and loss of function mutations are found in some lipodystrophy patients. We set out to understand the role of ARL15 in adipogenesis and showed that endogenous ARL15 palmitoylated and localised in the Golgi of mouse liver. Adipocyte overexpression of palmitoylation-deficient ARL15 resulted in redistribution to the cytoplasm and a mild reduction in expression of some adipogenesis-related genes. Further investigation of the localisation of ARL15 during differentiation of a human white adipocyte cell line showed that

ARL15 was predominantly co-localised with a marker of the cis face of Golgi at the preadipocyte stage and then translocated to other Golgi compartments after differentiation was induced. Finally, co-immunoprecipitation and mass spectrometry identified potential interacting partners of ARL15, including the ER-localised protein ARL6IP5. Together, these results suggest a palmitoylation dependent trafficking-related role of ARL15 as a regulator of adipocyte differentiation via ARL6IP5 interaction.

Introduction

The World Health Organisation (WHO) estimates there were 422 million people with diabetes in 2014. Approximately 90% of people with diabetes have Type 2 diabetes (T2D) that is characterised by defects in insulin secretion and insulin action. Increased body mass index (BMI), leading to insulin resistance, is one of the key determinants of lifetime T2D risk (Hippisley-Cox et al., 2009; Narayan et al., 2007). Genome wide association population studies have identified over 243 genetic loci with 403 distinct association signals for T2D (Mahajan et al., 2018). Although many of these loci indicate a role for islet beta-cell function in T2D risk, 26 signals were attenuated by BMI adjustment suggesting T2D risk was driven by adiposity. A further 15 loci were more strongly associated with BMI-adjusted signals with effects on insulin secretion and/or ectopic fat storage (Mahajan et al., 2018). Importantly, there is also genetic evidence of insulin resistance in T2D that is linked to ectopic fat distribution and reduced subcutaneous adiposity (Scott et al., 2014; Yaghootkar et al., 2014). In addition there are rare monogenic conditions such as lipodystrophy that result in partial or complete loss of adipose tissue and cause severe insulin resistance and diabetes (Semple et al., 2011).

The small GTPase adenosine diphosphate (ADP)-ribosylation factor-like protein 15 (ARL15) gene locus is associated with several metabolic traits including increased risk of T2D, lower adiponectin and higher fasting insulin levels (Richards et al., 2009). This gene locus was also associated with insulin resistance and adiposity (Scott et al., 2014, 2012; Yaghootkar et al., 2014). Further, loss of function mutations in the *ARL15* gene have also been identified in lipodystrophy patients (Rocha et al., 2017). These associations suggest a role for ARL15 in adipose tissue homeostasis. Indeed, it has been shown that reduction of *Arl15* impaired adipogenesis in 3T3-L1 pre-adipocytes and reduced adiponectin secretion from mature adipocytes (Rocha et al., 2017). Additionally, it has been shown that siRNA-mediated *ARL15* depletion in a human β cell line (EndoC-βH1) reduces insulin secretion, further linking this

gene to diabetes traits (Thomsen et al., 2016). However, the mechanisms by which ARL15 potentially regulate these processes remain unknown.

The family of ADP-ribosylation factor-like proteins (ARL) belong to the small GTPases RAS superfamily that exhibit structural homologies such as the inter-switch toggle and that switch between GTP-bound active and GDP-bound inactive conformations (D'Souza-Schorey and Chavrier, 2006; Kahn et al., 2006). ARF family proteins are largely involved in membrane trafficking and membrane-associated metabolic regulation (Burd et al., 2004; D'Souza-Schorey and Chavrier, 2006; Nie et al., 2003) and ARL family proteins have more diverse subcellular localisations and functions (Burd et al., 2004). For example, activated ARL1 and ARL3 are localised at the trans-Golgi network (TGN) and regulate Golgi trafficking pathways by recruiting Golgi targeting proteins such as the GRIP domain (Panic et al., 2003; Setty et al., 2003); whereas centrosome localised ARL2 and ARL3 play roles in regulating cell morphology and cell cycle by manipulating microtubule-related pathways (C. Zhou et al., 2006). In cilia, ARL13B is likely to regulate post-translational modification of tubulin (Larkins et al., 2011). Adipogenesis is a well-regulated multi-step process that is comprised of cell growth arrest, transcriptional activation, morphological changes and Golgi-mediated membrane vesicle trafficking (Tang and Lane, 2012). In addition to showing that ARL15 is an adipogenic regulator (Rocha et al., 2017), overexpression of ARL4D another family member, in 3T3-L1 cells reduced expression levels of several important adipogenesis-related genes such as aP2 (FABP4), fatty acid synthase (FASN), lipoprotein lipase (LPL) and hormone-sensitive lipase (HSL) (Yu et al., 2011), indicating a negative regulatory role of ARL4D on adipogenesis.

In this study, in order to investigate the mechanistic role of ARL15 in regulating adipocyte differentiation, we first investigated endogenous subcellular localisation, post-translational modification and localisation change of ARL15 during adipogenesis. Secondly, we explored potential protein-protein interacting partners of ARL15. These results provide useful information on ARL15 during adipogenic differentiation.

Results

Endogenous ARL15 is predominantly localised in the Golgi network
Using a protein over-expression method, the localisation of GFP-tagged ARL15 in 3T3-L1 preadipocytes has been shown in the Golgi network (Rocha et al., 2017); whereas in C2C12 myotubes, ARL15 was found to be in the cytoplasm and moved to the perinuclear Golgi

region upon insulin stimulation (Zhao et al., 2017). Therefore, we first sought to confirm the localisation of endogenous ARL15 in a purified Golgi network fraction isolated from mouse liver. Western blotting showed that, at steady state, ARL15 was enriched in the Golgi fraction together with a known Golgi marker RCAS1 (**Fig. 1A**) but not in the visible lipid fraction. We then conducted immunostaining in human white adipocyte tissue derived cell line (hWAT) preadipocytes to confirm the localisation of endogenous ARL15. Immunostaining showed the co-localisation of ARL15 with 58kDa protein, a known Golgi membrane-associated protein (Bloom and Brashear, 1989; Gao et al., 1998), in the perinuclear region (**Fig. 1B**). Together, these results clearly demonstrate that endogenous ARL15 is predominantly localised in Golgi.

Endogenous palmitoylated ARL15 is localised in the Golgi network

Palmitoylation is an important form of post-translational modification (PTM) that regulates protein subcellular localisation, Endoplasmic Reticulum (ER)-Golgi trafficking and protein-protein interaction (Aicart-Ramos et al., 2011). ARL15 has been identified as a putative palmitoylated protein by mass spectrometry from a human T lymphocyte cell line (Jurkat T cells) (Martin and Cravatt, 2009), mouse adipose tissue and 3T3-L1 adipocytes (Ren et al., 2013). To validate this, a resin-assisted capture (RAC) assay was conducted to first pull down a known palmitoylated protein ARL13B in mouse inguinal white adipose tissue (iWAT). Palmitoylated ARL13B was detectable in the pulldown sample by labelling with anti-ARL13B antibody (**Supplementary Fig. 1**). In agreement with the mass spectrometry findings (Ren et al., 2013), palmitoylated ARL15 was detectable in the pulldown sample by labelling with anti-ARL15 antibody (**Fig. 1C**).

Several important palmitoyl transferases that regulate the palmitoylation process have been found in Golgi (Aicart-Ramos et al., 2011) and ARL15 had been found to be predominantly localised in Golgi. To examine if palmitoylated ARL15 is localised in Golgi, the RAC assay was carried out in the Golgi fraction isolated from mouse liver, where ARL15 is also strongly expressed. Indeed, palmitoylated ARL15 was detectable in the pulldown sample from Golgi fraction by labelling with anti-ARL15 antibody (**Fig. 1D**).

Palmitoylation is required for ARL15 to establish its predominant Golgi network localisation

In addition to palmitoylation, prenylation and myristoylation modifications mediate subcellular localisation, protein-protein or protein-membrane interactions (Aicart-Ramos et al., 2011). However, whether ARL15 is prenylated or myristoylated remains unclear. To explore the possibility of ARL15 prenylation, the amino acid sequence of mouse ARL15 was analysed by

Prenylation Prediction Suite (PrePS: http://mendel.imp.ac.at/sat/PrePS/index.html). ARL15 neither has a cysteine on the fourth last position as part of a C-terminal CaaX box nor a cysteine within the last five positions of its C-terminal end, and is therefore unlikely to be subject to prenylation processes including CaaX Farnesylation, CaaX Geranylgeranylation or Rab Geranylgeranylation. To predict ARL15 myristoylation, the amino acid sequence of mouse ARL15 was analysed by Myristoylator from ExPASy Bioinformatics Resource Portal of Swiss Institute of Bioinformatics (Artimo et al., 2012). Due to a lack of a glycine residue at its N-terminal end, ARL15 was predicted not to be myristoylated.

ARL15 has three palmitoylation sites at its N-terminal (Cys17, Cys22 and Cys23) predicted by a clustering and scoring strategy algorithm CSS-Palm 4.0 (**Supplementary Table 1**) (Xue et al., 2011; F. Zhou et al., 2006). To test if these cysteine residues are important for the Golgi localisation of ARL15, the three cysteine (C) residues were mutated to tyrosine (Y) through site-directed mutagenesis. The C-terminal Myc tagged wild type (WT) or N-terminal mutant *Arl15* constructs (C17Y, C22Y, C23Y, C22Y/C23Y and C17Y/C22Y/C23Y) were over-expressed in 3T3-L1 preadipocytes. Subcellular localisation of WT and mutant ARL15 was studied using immunostaining and confocal microscopy. Consistent with endogenous ARL15, over-expressed wild type ARL15 was predominantly if not exclusively localised in Golgi (**Fig. 2A**) (Rocha et al., 2017). Similarly, the C17Y mutant was also localised in Golgi (**Fig. 2B**) with some plasma membrane accumulation. In contrast to the predominant Golgi localisation of ARL15 the C22Y, C23Y, C22Y/C23Y and C17Y/C22Y/C23Y mutants, each exhibited a cytoplasmic diffused pattern (**Fig. 2C-H**).

To further prove that mutant ARL15 disrupted Golgi localisation is due to the palmitoylation defect per se and not due to effects such as misfolding or abnormal degradation of the mutant protein we treated 3T3-L1 cells with 2-bromopalmitate (2-BP), a non-metabolizable palmitate analogue that blocks palmitate incorporation onto proteins. To validate that 2-BP sufficiently inhibits palmitoylation of ARL15, we performed an S-palmitoylation acyl-RAC assay. In cells treated with 100μM 2-BP overnight, ARL15 was detected in the input fraction and significantly reduced in the pull-down fraction indicating inhibition of palmitoylation compared to the non-treated control cells (**Supplementary Fig 2A-B**). The same was observed for ARL13B, a known palmitoylated protein included as a positive control (**Supplementary Fig 2C**). In order to test the effect of 2-BP inhibition of palmitoylation on ARL15 localisation we transfected 3T3-L1 cells with the C-terminal Myc tagged wild type (WT) or the or C-terminal mutant *Arl15* construct C22Y/C23Y and then treated the WT with or without 2-BP. Immunofluorescence analysis revealed that WT ARL15 expressing cells treated with 2-BP and mutant C22Y/C23Y expressing cells comprised a cytoplasmic and

non-specific Golgi (58KDa protein cis-Golgi marker) localisation (**Fig. 3A-C, G-I**). Co-staining with calreticulin an endoplasmic reticulum (ER) marker revealed again that WT ARL15 is not ER exclusively localised but rather localised in a distinct region reminiscent of Golgi (**Fig 3D**). In contrast, WT ARL15 expressing cells treated with 2-BP and cells expressing C22Y/C23Y lost this distinct localisation and appeared to correlate more with ER (**Fig 3D-F, G-I**). These immunostaining data indicated that residues Cys22 and Cys23 are essential for ARL15 Golgi localisation. However, they do not directly show that these residues are the palmitoylation sites. In order to prove show this and validate the predictive algorithm for residues Cys22 and Cys23 we performed an S-palmitoylation acyl-RAC assay in 3T3-L1 cells expressing either the WT ARL15 protein or the mutant C22_C23 protein. WT ARL15 was detected both in the input and the pull-down fraction whereas C22Y/C23Y mutant protein was only present in the input fraction, indicating loss of palmitoylation in these residues unlike ARL13B which was detected in the pull-down fraction of the mutant protein (**Fig. 3J**). Taken together, these findings show that Cys22 and Cys23 are the sites of palmitoylation and that this post translational modification is important for ARL15's Golgi localisation.

ARL15 translocates away from Golgi network membranes during adipogenesis

Since palmitoylation is a dynamic and reversible membrane association process (Conibear and Davis, 2010), it is probable that ARL15 is not permanently restricted to membrane structures. To study whether the association between ARL15 and intracellular membrane changes during adipogenesis, total 3T3-L1 cell lysate and membrane-enriched fractions from pre-adipogenic (D-3, D0) and post-adipogenic (D4, D12) stages (D0: differentiation induction) were subjected to western blot analysis. Adiponectin was used as a mature adipocyte marker and as expected its protein level was considerably increased at the late adipogenic stage (D12 post-differentiation) (**Fig. 4A**). During adipogenesis, changes in protein levels of ARL15 in the membrane-enriched fraction exhibit a different trend compared to those in the total cell lysate; whereas the Golgi marker RCAS1 did not show such difference (**Fig. 4A**). The level of ARL15 (relative to GAPDH) in the membrane-enriched fraction was significantly reduced at the late stage of adipogenesis (D12, post-differentiation) compared to earlier time points (**Fig. 4B**), suggesting that ARL15 dissociates from the membrane at a late stage of adipogenesis. Having observed changes in cellular localisation of ARL15 during adipocyte differentiation we wanted to further investigate the palmitoylation status of the protein during this process. Therefore, we performed an S-palmitoylation acyl-RAC assay over the time course of adipogenesis in 3T3L-1 cells. In agreement with the previous observation of ARL15 palmitoylation there was a trend towards reduction between post-adipogenic time point D4 and D12 (p=0.06) (**Fig. 4C-D**) although this was not statistically significant possibly due to variation between multiple repeats in this assay.

Since ARL15 is predominantly co-localised with the Golgi network membrane protein 58kDa protein in preadipocytes, we next asked if ARL15 changes its sub-Golgi localisation during the adipocyte differentiation process in hWAT cells. Cells at pre-adipogenic and post-adipogenic stages (D0, D5, D10 and D15 post-differentiation induction) were subjected to immunostaining. We found that in hWAT preadipocytes (D0), endogenous ARL15 is co-localised with Golgi marker 58kDa protein (**Fig. 4E**), consistent with previous findings. However, after the induction of adipogenesis, we found that the Golgi network changed from its canonical stack of tubular structures to a ring shape. ARL15 was then no longer co-localised with the 58kDa protein and became confined within the Golgi ring. This localisation remained unchanged even 15 days post differentiation (**Fig. 4E**), suggesting that although predominantly localised in Golgi, ARL15 changes its sub-Golgi localisation during adipogenesis.

As the recycling endosome is also spatially confined within the Golgi ring (Misaki et al., 2007), we tested whether ARL15 is also localised in the recycling endosome and trafficked away from Golgi. We co-stained hWAT cells at pre-adipogenic and post-adipogenic stages (D0, D5, D10 and D15 post-differentiation induction) with ARL15 and the recycling endosome marker VAMP3. We found that VAMP3 was distributed in both Golgi area and in the cytoplasm (**Fig. 5A**). The cytoplasmic VAMP3 exhibits small punctate morphology, likely to reflect the previous finding that VAMP3 is localised in both recycling and early endosome (Galli et al., 1994; McMahon et al., 1993). Pearson's correlation coefficients (PCC) were used to assess the degree of colocalisation between ARL15 and VAMP3. PCC was significantly higher at D5 than other time points (**Fig. 5B**), suggesting that ARL15 transiently colocalises with VAMP3 during early stages of adipogenesis. In addition, the co-localisation was only visible within the Golgi area, not in small punctate cytoplasmic-distributed structures (**Fig. 5A**), suggesting that ARL15 stays in Golgi network area during adipogenesis.

To exclude the possibility of ARL15's localisation in early endosome, hWAT cells at D0, D5, D10 and D15 post-differentiation induction were co-stained with ARL15 and an early endosome marker EEA1 (**Supplementary Fig. 3**). However, co-localisation was not seen at any time points between D0 and D15 as evaluated by Pearson's coefficients, which were all below 0.25, suggesting the two proteins are unlikely to colocalise and that ARL15 does not localise in early endosome **(Fig. 5C)**.

Arl15 overexpression reduces levels of late-stage adipogenesis-related genes

To study potential effects of *Arl15* overexpression in adipogenesis and roles that ARL15 palmitoylation may play on adipocyte differentiation, C-terminal Myc tagged empty vector control, *Arl15* WT or mutant (C17Y/C22Y/C23Y) was expressed from a human cytomegalovirus (CMV) in 3T3-L1 cells prior to adipogenesis and gene expression analysis carried out on cells over a differentiation time-course at D0 (2 days post transfection) and at D4 and D7 post differentiation induction **(Supplementary Fig. 4 and Fig. 6A-I)**. The levels of *Arl15* over-expression were assessed using two different TaqMan probes targeting exons 1-2 and 3-4 of WT *Arl15* (NCBI Reference Sequence: NM_172595.4), respectively. As expected, qPCR confirmed a significant over-expression of *Arl15* WT by both TaqMan probes at D0 compared to the empty vector control (**Fig. 6A & B**), whereas in the *Arl15* mutant group, the probe that only covers the non-mutation-containing exon 3 and 4 can detect a similar level of over-expression (**Fig. 6B**), demonstrating successful expression of both WT and mutant *Arl15*. The master adipogenesis regulator *Pparγ* showed upregulation in *Arl15* WT in comparison to empty vector at D0 and upregulation in mutant compared to *Arl15* WT expressing cells at day 7 (**Fig. 6FD).** The mature adipocyte marker adiponectin (*AdipoQ*) showed some upregulation at D4 comparing both WT and mutant overexpressing cells to empty vector but not at the later time point (**Fig. 6F**). The fatty acid synthase (*Fasn*) gene showed some evidence of reduction in mutant cells compared to WT at D0 but not at other timepoints (**Fig. 6G**). The early adipogenesis-related gene CCAAT enhancer binding protein alpha (*Cebpα*) and markers of differentiation, Fatty Acid Binding Protein 4 (*Fabp4),* glucose transporter type 4 (*Glut4*) and perilipin1 (*Plin1)* showed no differences although there may be a trend (p=0.0664) for reduction of *Plin* 1 in WT compared to empty vector (**Fig. 6C, E, H and I**).

Cytoplasmic lipid droplet levels were also tested using Oil Red O staining at D7. There were no significant differences detectable in either *Arl15* WT or mutant group, comparing to the empty vector control (data not shown). Taken together, these results show that *Arl15* WT or mutant over-expression only impaired adipogenesis to a limited extent.

ARL15 interacts with ARL6IP5

The Golgi network is the hub of vesicle trafficking and protein-protein interactions. To identify interacting partners of ARL15, immunoprecipitation (IP) was carried out using an anti-ARL15 antibody to pull down ARL15 from brain lysate from wildtype and homozygous KO mice (**Fig. 7A**), wildtype subcutaneous adipose tissue lysate (**Fig. 7B**) and 3T3-L1 cells at different timepoints during adipogenesis (D-3, D0 and D4 post differentiation induction) (**Fig. 7C**). Western blotting demonstrated successful pull-down of ARL15, as the ARL15 protein band

was only detectable in the pull-down lanes, not in control IgG or knockout mouse tissue lanes (**Fig. 7A-C**). Potential protein-protein interacting complexes from whole immune-precipitation samples were then analysed by mass spectrometry. Several interacting partners were identified (**Table 1**). Among them, ADP Ribosylation Factor like GTPase 6 Interacting Protein 5 (ARL6IP5) also named as JWA and GTRAP3-18 was identified as a potential interacting partner of ARL15 in all samples. Importantly, for mouse brain lysate, homozygous *Arl15* knockout mouse brain was used as a negative control for the western blot and mass spectrometry analysis instead of IgG, excluding the possibility of antibody non-specificity. ARL6IP5 was detectable by mass spectrometry only in WT mouse brain lysate pulled down by anti-ARL15 antibody, not in the homozygous *Arl15* knockout control (**Table 1**), further suggesting that ARL6IP5 is a potential interacting partner of ARL15. To confirm the interaction between ARL15 and ARL6IP5, WT mouse brain lysate was subjected to immunoprecipitation followed by western blotting. ARL6IP5 bands were detectable in ARL15 pulled-down samples, but not in the IgG control, demonstrating the interaction between ARL15 and ARL6IP5 (**Fig. 7D**). Of note, only dimer and multimer forms of ARL6IP5 were detectable, consistent with previous findings that ARL6IP5 also exists as non-monomeric forms in the brain and other cell types (Lin et al., 2001; Vento et al., 2010).

Discussion

In the present study, results from immunocytochemistry demonstrated that both endogenous ARL15 in hWAT preadipocytes and overexpressed WT ARL15 in 3T3-L1 preadipocytes co-localised with the Golgi network and in colocalising with 58kDa Golgi protein likely faced the cytosol (Bloom and Brashear, 1989).

Previously, Ren *et al.* conducted proteomic analysis and showed that two ARL family proteins, ARL3 and ARL15, were palmitoylated in adipose tissues (Ren et al., 2013). Using stable isotope labelling by amino acids in cell culture (SILAC), ARL15 was also found to be palmitoylated in human umbilical vein endothelial cells (HUVECs) (Wei et al., 2014). Using the acyl-RAC assay, we have confirmed palmitoylation of ARL15 in mouse adipose tissue and Golgi isolated from mouse liver. Numerous peripheral membrane proteins have been found to be palmitoylated at the surface of Golgi (Rocks et al., 2010), while palmitoylated integral membrane cargo proteins are found to be in the rims of cis-Golgi (Ernst et al., 2018), suggesting that sub-Golgi localisation may be important to a protein's function. Since the hydrophobic palmitoyl group enables a reversible protein-membrane association this may facilitate reversible association of ARL15 with Golgi membranes (Charollais and Van Der Goot, 2009; McLaughlin and Denny, 1999). Indeed, we found that in hWAT cells, ARL15

was translocated away from Golgi surface, suggesting a potential depalmitoylation process after adipogenic induction, consistent with a role for ARL15 in protein and membrane trafficking in adipocytes. Interestingly, a number of proteins involved in lipid formation and metabolism are also palmitoylated (Ren et al., 2013). ARL15 has been reported to be translocated from the cytoplasm to Golgi around the nucleus on insulin stimulation of muscle C2C12 cells (Zhao et al., 2017), however our immunostaining data demonstrated that in the absence of insulin stimulation, both endogenous ARL15 in hWAT preadipocytes and over-expressed ARL15 in 3T3-L1 preadipocytes were also established at a perinuclear Golgi localisation. These may be cell specific differences.

To date, the significance of ARL15 palmitoylation in adipogenesis remains to be elucidated. In our study, 3T3-L1 cells over-expressing WT and palmitoylation mutant *Arl15* (C17_22_23) were differentiated and there was some evidence of upregulation of the adipogenesis master regulator *Pparγ* at early and late timepoints and an upregulation of the mature differentiation *AdipoQ* at day 4 in both WT and mutant cells. Conversely there was a reduction in the differentiation marker *FASN,* in mutant cells although this was only at an early timepoint where expression is expected to be low. However, it should be noted that not all cells are likely to be overexpressing ARL15 in these transfection experiments. A more direct test of the importance of palmitoylation in adipogenesis would be possible using engineered cells expressing endogenous levels of ARL15.

Links between palmitoylation of other ARL family proteins and adipogenic regulation have been observed. For instance, ARL13B has palmitoylation-dependent roles on cilia formation and Sonic hedgehog (Shh) pathway regulation (Larkins et al., 2011; Roy et al., 2017). Shh protein treatment on 3T3-L1 and NIH-3T3 cells inhibited adipogenesis, demonstrating a negative regulatory role of Shh pathway on adipogenesis (Suh et al., 2006). Additionally, cilia carrying hedgehog pathway proteins transiently appeared in human white preadipocyte (HWP) during adipogenesis, whereas cilia deformation resulted in upregulation of adipogenic master regulator PPARγ (Bangs and Anderson, 2017; Marion et al., 2009).

Two important adipose proteins, the hormone adiponectin and the glucose transporter GLUT4, have also been shown to be palmitoylated in adipose tissue (Ren et al., 2013). Overexpression of a palmitoylation mutant (Cys223) of GLUT4 resulted in change of subcellular localisation and impairment of insulin dependent membrane translocation (Ren et al., 2015), suggesting an important role for palmitoylation in facilitating membrane trafficking of GLUT4. However, ARL15 does not appear to be directly involved in trafficking of adiponectin or GLUT4, as adiponectin was not colocalised with ARL15 as reported by Rocha

et al. (Rocha et al., 2017) and in our co-immunoprecipitation experiments we also did not find evidence of direct interaction between adiponectin or GLUT4 proteins in mouse iWAT. Further, 5 days after induction of adipogenesis, we could not immunocytochemically detect co-localisation between ARL15 and GLUT4 in hWAT cells incubated in insulin-containing medium. Similarly, Rocha *et al.* found that knocking down *Arl15* had little impact on GLUT4 translocation-mediated glucose uptake (Rocha et al., 2017).

Other Golgi localised ARL family proteins, for example, ARL1, ARL5 and ARL18 (ARFRP1) are all mediators of vesicle/membrane trafficking and transport (Houghton et al., 2012; Lowe et al., 1996; Shin et al., 2005) and is a plausible role for ARL15. However, the cargo specificity and relationship between the Golgi localisation of palmitoylated ARL15 and intracellular trafficking needs to be further studied.

A novel protein-protein interacting partner of ARL15 has been reported. Using Co-IP followed by mass spectrometry, a pioneer study revealed that the ArfGAP protein containing a SH3 Domain, Ankyrin Repeat And PH Domain 2 (ASAP2) interacts with ARL15 (Zhao et al., 2017). However, ASAP2 was identified from C2C12 skeletal muscle cell samples where insulin-mediated translocation of ARL15 to Golgi was detected; whereas in our 3T3-L1 or hWAT samples, such translocation was not seen, suggesting potentially different interacting partners. Indeed, we did not identify ASAP2 by mass spectrometry from Co-IP 3T3-L1 samples at different adipogenic timepoints or from mouse iWAT lysate. We identified ARL6IP5 as an interacting partner of ARL15 not only in adipose-related cell types and tissue, but was also in brain samples, indicating common pathways that ARL15 may be involved in brain and adipose tissue. Predominantly localised in ER (Maier et al., 2009), ARL6IP5 has been found to reduce ER-Golgi trafficking by interacting with ER-Golgi transport regulator RAB1 and such interaction exhibited an inhibitory effect on neuronal differentiation (Maier et al., 2009). Since our results revealed that ARL15 is likely to be localised at the ER-facing cis Golgi network, such localisation indicates that ARL15 may be involved in mediating ER-Golgi transport via interacting with ARL6IP5. In addition to the potential role of ARL6IP5 in regulating neuronal differentiation, knocking down *Arl6ip5* in UAMS-32 osteoblastic cell line has been reported to reduce cell proliferation and differentiation (Wu et al., 2014). Such a role is consistent with a regulatory role in adipocyte differentiation (Rocha et al., 2017).

In conclusion, we demonstrated that endogenous ARL15 is palmitoylated in subcutaneous adipose tissue and palmitoylation seems to be involved in maintaining the Golgi localisation of ARL15. ARL15 interacts with ARL6IP5 an ER-localised protein and translocates within the Golgi network during adipogenic differentiation consistent with a role in protein trafficking.

Taken together, these results indicated a palmitoylation dependent Golgi-based role of ARL15 as a regulator of cell differentiation.

Material and methods

Primers and cloning

Primers used for the site-directed mutagenesis were synthesised by Sigma-Aldrich and pCMV-Arl15-Myc-DDK vector was used as a template. Primer sequences are: C17Y: forward: 5'-ATGGATTATCTATGTTTTCGAGCG-3', and a reverse: 5'-GTACAGAAACGCCTCAGTTATC-3'; C22Y: forward:-5'-GCTTTACTGCAAGGGACCAC-3', and a reverse: 5'- GCTCGAAAACACAGATAATCC-3' ;C23Y: forward: -5'-GCTTTGCTACAAGGGACCAC-3' and reverse: 5'- GCTCGAAAACACAGATAATCC-3' ;C22_23Y: forward: 5'- GCTTTACTACAAGGGACCAC-3', and reverse: 5'-GCTCGAAAACACAGATAATCC-3'. Site-directed mutagenesis and Kinase, Ligase & DpnI (KLD) treatment were conducted using Q5® Site-Directed Mutagenesis Kit as per the manufacturer's instruction. Transformation was carried out by mixing a 50 μl of NEB 5-α Competent *E.coli* with 5 μl of the KLD product and placed on ice for 30 minutes. Then, the mixture was heat shocked at 42°C for 30 seconds followed by placing on ice for 5 minutes. 950 μl of room temperature SOC was pipetted into the mixture followed by a 60-minute incubation at 37°C, 250 rpm. Then, 50-100 μl of the transformation mix in SOC was plated onto a kanamycin selection plate and incubated overnight at 37°C. Constructs were verified by Sanger sequencing.

Cell culture

3T3-L1 (ATCC, CL-173) or human white adipocyte (hWAT, provided by Prof Yu-Hua Tseng, PhD at Harvard Medical School, Joslin Diabetes Center, Boston, MA 02215 (Xue et al., 2015)) cells were maintained in Dulbecco's Modified Eagle's Medium (DMEM) with glucose, containing L-glutamine and supplemented with 10% NBCS or FBS and 1% Penicillin-streptomycin mixture (Life Technologies) at 37°C, 5% CO2. Cells were checked for mycoplasma and were negative. Cells at different passage were used as replicates. To induce adipogenesis in 3T3-L1 preadipocytes, differentiation medium containing DMEM (ThermoFisher, CAT No 31966021) supplemented with 10% FBS, 1% Penicillin-streptomycin mixture (Life Technologies), 500 μmol/L IBMX, 1 μmol/L dexamethasone, 10 μmol/L insulin was added to 2-day post-confluent 3T3-L1 preadipocytes and cultured for 4 days. Cells were further cultured in maintenance medium containing DMEM supplemented with 10% Tet-Approved FBS, 10 μmol/L insulin (Merck, CAT No I9278) until harvest for

analysis. Adipogenesis induction in hWAT cells was adapted from Xue *et al.* with modifications (Xue et al., 2015). In brief, differentiation medium containing DMEM (ThermoFisher) supplemented with 2% FBS, 1% Penicillin-streptomycin mixture (Life Technologies), 2 nmol/L T3, 33 μmol/L biotin, 17 μmol/L pantothenate, 30 μmol/L indomethacin, 0.5 mmol/L IBMX, 0.1 μmol/L dexamethasone and 0.5 μmol/L insulin was added to post-confluent hWAT preadipocytes and cultured until harvest for analysis

Golgi network isolation

Golgi isolation was carried out by using a Golgi isolation kit (Sigma-Aldrich) as per manufacture's instruction with minor modifications. Mouse liver tissue was first washed with ice-cold PBS, then washed once with 10 ml of 0.25 M Sucrose Solution and weighed. The tissue was then minced with scissors. The minced tissue was then suspended with 1 ml of the 0.25 M Sucrose Solution per 1 g of tissue. Tissue suspension was then transferred into a homogenisation tube and homogenised with 6 slow motions of the PTFE pestle at 300 rpm. The homogenate was then centrifuged at 3,000 ×g for 15 minutes at 2–8 °C. After centrifugation, the supernatant was transferred to a fresh tube. The sucrose concentration in the supernatant was calculated according to Equation (1): [Sucrose] = 0.25*Buffer Volume/ (Tissue Weight + Buffer Volume). Where: [Sucrose] is the molar sucrose concentration in the supernatant; 0.25 is the molar sucrose concentration in the homogenization buffer; Buffer Volume is the volume (ml) of the buffer used to re-suspend tissue after mincing; Tissue Weight is the weight of tissue in grams. The volume of the 2.3 M Sucrose Solution to be added to the supernatant to obtain a final sucrose concentration of 1.25 M was calculated according to Equation (2): Sucrose Volume = Sup Volume *(1.25−[Sucrose])/1.05. Where: Sucrose Volume is the volume (ml) of 2.3 M Sucrose Solution to be added to the supernatant in order to obtain a final concentration of 1.25 M sucrose; Sup Volume is the volume (ml) of the supernatant; [Sucrose] is the molar sucrose concentration in the supernatant from Equation (1). 1.05 is the difference in the molarity between the sucrose stock solution (2.3 M) and the sucrose concentration of the sample (1.25 M).

After calculation, the sucrose concentration in the sample (supernatant) was adjusted to 1.25 M by adding the volume of 2.3 M Sucrose Solution calculated in Equation (2). The solution was mixed by inverting the tube followed by a brief vortex. A discontinuous gradient in an ultracentrifuge tube was then made. The order of sucrose gradient fractions in the tube (from bottom to top) were: 1.84 M Sucrose Solution, sample (sucrose concentration adjusted to 1.25 M), and 1.1 M Sucrose Solution and 0.25 M Sucrose. The tubes were then centrifuged at 120,000 ×g for 3 hours at 4°C. The Golgi enriched fraction was at the 1.1 M/0.25 M sucrose interphase.

Protein extraction, antibodies and western blotting

3T3-L1 cells were lysed in M-PER™ Mammalian Protein Extraction Reagent (ThermoFisher Scientific), mouse tissues were lysed in T-PER Tissue Protein Extraction Reagent (ThermoFisher Scientific) as per manufacturer's instructions, supplemented with protease and phosphatase inhibitors (Roche). Protein concentrations of lysates were measured against a serial dilution of BSA standards using the *DC*™ (detergent compatible) protein assay (Bio-Rad). 10µl of 4X LDS Sample loading buffer (Life Technologies) and 4µl of 10X reducing agent (Life Technologies) were added to 20 µg of protein lysates, heat-denatured at 95°C for 5 minutes and then loaded on 4%-12% Bis-Tris NuPAGE precast gels (Life Technologies). Proteins were transferred to 0.45µm PVDF membranes (GE) using the XCell II™ Blot module (Life Technologies). Membranes were first incubated in blocking solution (5% dried non-fat milk prepared in Tris-buffered saline containing 0.1% Tween-20 (TBST)) at room temperature for an hour on a shaking platform, washed with TBST and then incubated with primary antibodies overnight at 4°C on a shaking platform. The membranes were washed three times with TBST and finally incubated with HRP-conjugated anti-rabbit or anti-mouse (BioRad), secondary antibody prepared in blocking solution for 1 hour at room temperature. After washing excess antibody, the Pierce™ ECL Plus Western Blotting Substrate was used for signal detection using the UVP ChemiDoc-It™ Imaging System.

The following antibodies were used: rabbit anti-ARL15 (Abcam ab178425, 1:1,000), mouse anti-GAPDH (Abcam ab8245, 1:10,000), mouse anti-adiponectin (Abcam ab22554, 1:1,000), mouse anti-ARL13B (Abcam ab136648, 1:200), mouse anti-RCAS1 (Cell Signaling #678565, 1:1,000) and rabbit anti-ARL6IP5 (Sigma-Aldrich SAB1306837, 1:1,000).

Quantitative real time PCR (qPCR)

RNA was extracted from 3T3-L1 cells using Direct-zol RNA Kit (Zymo Research) as per the manufacturer's instructions and the concentration measured using a Nanodrop system. cDNA was generated using Superscript III reverse transcriptase enzyme (Life Technologies) and analysed by qPCR using the TaqMan system based on real-time detection of accumulated fluorescence (ABI Prism 7700, Perkin-Elmer Inc., USA). Samples were tested in triplicate and gene expression normalised relative to the expression of house-keeping genes *CanX* (Mm00500330_m1) and *Rpl13a* (Mm01612986_gH). *Arl15* (Mm01304728_m1 Exon1-2 and Mm00553694_m1 Exon 3-4), *C/ebpα* (Mm00514283_s1), *C/ebpβ* (Mm00843434_s1), *Pparγ* （Mm01184322_m1, *Fabp4* （Mm00445878_m1）, *Glut4* (Mm00436615_m1), *AdipoQ* （Mm00456425_m1), *Plin1* (Mm00558672_m1**)** and *Fasn* (Mm00662319_m1) FAM labelled TaqMan Probes were purchased from Applied Biosystems (ABI, USA).

Immunofluorescence

Cells were grown on coverslips in 12-well plates. After washing with PBS, cells were fixed using 4% PFA and permeabilised using 0.1% Triton X-100 (Sigma). To block non-specific antibody binding, cells were blocked for 1 hr at room temperature in blocking buffer containing 5% donkey serum, Tween-20 (Bio-Rad) and Glycine (Sigma). Staining was carried out using primary antibodies with optimised concentrations overnight at 4°C followed by 3 washes with PBST. Alexa fluorophore conjugated secondary antibodies were used to detect primary antibody-labelled proteins for 1 hour at room temperature. DNA stain NucBlue present in mounting medium (Thermo, P36985) or DAPI was used to stain cell nuclei. DAPI stained cells were mounted onto slides using the DAKO fluorescent mounting medium. Cells were imaged on the Zeiss inverted confocal microscope (Carl Zeiss, Switzerland)

Primary antibodies used: rabbit anti-ARL15 (Sigma-Aldrich HPA063820, 1:100), rabbit anti-tagged Myc antibody (Abcam ab9106, 1:500), mouse anti-58kDa protein (Abcam ab27043, 1:100), mouse anti-VAMP3 antibody (Santa Cruz sc-514843, 1:100), mouse anti-EEA1 antibody (Abcam ab70521, 1:100), mouse anti-Myc (Invitrogen 132500, 1:200), rabbit anti-calreticulin (Abcam ab92516, 1:500). The following secondary antibodies were used: anti-mouse Alexa-568 (Thermo, A10037, 1:500) and anti-rabbit Alexa-488 (Thermo, A32790, 1:500) or goat anti-rabbit Alexa 488 (Abcam, ab150077, 1:1000) and goat a-mouse-Alexa 647 (Abcam, ab150115, 1:250).

Cell membrane enrichment

The cell membrane enrichment method was adapted from (Forrester et al., 2011) with minor modification. In brief, 3T3-L1 cells were collected and washed in cold PBS. After undergoing a freeze-thaw cycle, cells were resuspended in lysis buffer (25 mM HEPES, 25 mM NaCl, 1 mM EDTA, pH 7.5) containing protease inhibitor cocktail (Roche). Lysis was conducted by repeated passaging through a 28 gauge needle. Then cell lysates were centrifuged at 800 g for 5 min to get rid of nuclei and unbroken cells. The supernatant was then centrifuged at 20,000 g for 30 minutes at 4°C. The pellet was re-suspended in lysis buffer containing 0.5% Triton X-100. Total protein was quantified with a DC™ protein assay (Bio-RAD).

Acyl-RAC assay

Methodology for acyl-RAC, including blocking of free thiols with methyl methanethiosulfonate (MMTS) (Sigma-Aldrich, 208795-1G, Catalog number: 23011), pH 7.5), cleavage of thioester linkages, and capture of nascent thiols on thiopropyl sepharose, was from (Forrester et al., 2011) with minor modifications. In brief, equal amounts of protein (2.0 mg) were diluted to a concentration of 2 mg/ml in (total volume 1ml) blocking buffer (100 mM HEPES, 1.0 mM EDTA, 2.5% SDS, 0.1% MMTS, pH 7.5) and incubated at 40°C for 10

minutes with frequent vortexing. Three volumes of cold acetone were then added, and proteins were subjected to precipitation at −20°C for 20 minutes. Then the solution was concentrated at 5,000 g for 10 min, the pellet was extensively washed with 70% acetone, re-suspended in 300 µl of binding buffer (100 mM HEPES, 1.0 mM EDTA, 1% SDS, pH 7.5) and added to ~40 µl of prewashed thiopropyl sepharose beads (GE-Amersham). To this mixture was added 40 µl of either 2 M NH_2OH (freshly prepared in H2O from HCl salt and brought to pH 7.5 with concentrated NaOH) or 2 M NaCl. Binding reactions were carried out on a rotator at room temperature for 2–4 hours. Approximately 20 µl of each supernatant was saved as the "total input." Resins were washed at least five times with binding buffer. For immunoblot analysis, elution was performed using 60 µl of binding buffer containing 50 mM DTT at room temperature for 20 minutes. Supernatants were removed and mixed with Laemmli loading buffer, heated to 95°C for 5 minutes, and separated via SDS-PAGE on a Mini-Gel apparatus (Bio-Rad). For figures 3, 4 and supplementary figure 2, pull down of S-palmitoylated proteins was performed with the commercial kit CAPTUREome™ S-Palmitoylated Protein Kit (Badrilla, K010-311). Briefly proteins were extracted in 1X Binding Buffer A and were quantified by Pierce BCA protein kit assay (Thermo fisher). All proteins were then diluted to the same concentration. 50µL of each sample was then kept as the input fraction and the rest of the proteins were subjected to the resin-assisted capture assay according to the manufacturer's protocol.

Immunoprecipitation

3T3-L1 cells were lysed in M-PER™ Mammalian Protein Extraction Reagent (ThermoFisher Scientific), mouse tissues were lysed in T-PER Tissue Protein Extraction Reagent (ThermoFisher Scientific) as per manufacturer's instructions, supplemented with protease and phosphatase inhibitors (Roche) and 5mM $MgCl_2$ (Sigma-Aldrich). Protein G Sepharose beads (Sigma-Aldrich) were washed by 1ml lysis buffer and centrifuged at 1,000 g for 1 minute at 4°C. Cell or tissue lysates with the pre-washed beads were then incubated for 1 hour at 4°C followed by centrifugation at 1,000g for 1 minute at 4°C to remove the beads. Then antibody was added to the sample lysate. The antibody-containing pre-cleaned lysate was incubated on a tube rotator overnight at 4°C. After overnight incubation, freshly pre-washed Protein G Sepharose beads (Sigma-Aldrich) were added to the antibody-containing pre-cleaned lysate and incubated for 1 hour at 4°C. Then, beads were collected by centrifugation at 1,000g for 1 minute at 4°C followed by washing the immune complexes for 6 times using PBS supplemented with protease and phosphatase inhibitors to remove nonspecific binding. The protein-protein interacting partners were then eluted by boiling at 95°C for 5 minutes. Samples were then directly analysed by SDS-PAGE or stored at -20°C for subsequent use.

Mouse tissue samples

All animal studies were approved by the Medical Research Council Harwell Institute Animal Welfare and Ethical Review Board, and all procedures were carried out within project license restrictions (PPL 30/2642 and 30/3146) under the UK Animals (Scientific Procedures) Act 1986 and following the ARRIVE guidelines for animal research. Mice were housed according to UK Home Office welfare guidelines in a 12hr light / dark cycle at a temperature of 21± 2°C and humidity of 55 ± 10%. Mice were fed ad libitum and had free access to water (25 ppm chlorine). Tissue samples were obtained from C57BL/6Ntac and Arl15-Del2-EM1-B6N mice. The Arl15-Del2-EM1-B6N mice carry a 2-nucleotide CRISPR/Cas9 induced deletion in exon 2 of the *Arl15* gene and was generated by the Molecular and Cellular Biology team at the MRC Harwell Institute.

Statistical analysis

Statistical analysis was performed using the Graphpad Prism 8 software. Student's t-test, one or two-way ANOVA with repeated measures with post-hoc Tukey's correction was applied. P values ≤ 0.05 were considered significant. Data distribution normality was assessed by Shapiro-Wilk test (Graph Pad Prism 8). For equal variance assessment, F-tests were used and groups are with similar variance ($p > 0.05$).

References

Aicart-Ramos, C., Valero, R.A., Rodriguez-Crespo, I., (2011). Protein palmitoylation and subcellular trafficking. Biochim. Biophys. Acta **1808**, 2981–2994.

Artimo, P., Jonnalagedda, M., Arnold, K., Baratin, D., Csardi, G., de Castro, E., Duvaud, S., Flegel, V., Fortier, A., Gasteiger, E., et al., (2012). ExPASy: SIB bioinformatics resource portal. Nucleic Acids Res. **40**, W597-603.

Bangs, F., Anderson, K.V., (2017). Primary Cilia and Mammalian Hedgehog Signaling. Cold Spring Harb. Perspect. Biol. **9**, a028175.

Bloom, G.S., Brashear, T.A., (1989). A novel 58-kDa protein associates with the Golgi apparatus and microtubules. J. Biol. Chem. **264**, 16083–16092.

Burd, C.G., Strochlic, T.I., Setty, S.R.G., (2004). Arf-like GTPases: not so Arf-like after all. Trends Cell Biol. **14**, 687–694.

Charollais, J., Van Der Goot, F.G., (2009). Palmitoylation of membrane proteins (Review). Mol. Membr. Biol. **26**, 55–66.

Conibear, E., Davis, N.G., (2010). Palmitoylation and depalmitoylation dynamics at a glance. J. Cell Sci. **123**, 4007–4010.

D'Souza-Schorey, C., Chavrier, P., (2006). ARF proteins: roles in membrane traffic and beyond. Nat. Rev. Mol. Cell Biol. **7**, 347–358.

Ernst, A.M., Syed, S.A., Zaki, O., Bottanelli, F., Zheng, H., Hacke, M., Xi, Z., Rivera-Molina, F., Graham, M., Rebane, A.A., et al., (2018). S-Palmitoylation Sorts Membrane Cargo for Anterograde Transport in the Golgi. Dev. Cell **47**, 479-493.e7. 4

Forrester, M.T., Hess, D.T., Thompson, J.W., Hultman, R., Moseley, M.A., Stamler, J.S., Casey, P.J., (2011). Site-specific analysis of protein S-acylation by resin-assisted capture. J. Lipid Res. **52**, 393–398.

Galli, T., Chilcote, T., Mundigl, O., Binz, T., Niemann, H., De Camilli, P., (1994). Tetanus toxin-mediated cleavage of cellubrevin impairs exocytosis of transferrin receptor-containing vesicles in CHO cells. J. Cell Biol. **125**, 1015–1024. 5

Gao, Y.S., Alvarez, C., Nelson, D.S., Sztul, E., (1998). Molecular cloning, characterization, and dynamics of rat formiminotransferase cyclodeaminase, a Golgi-associated 58-kDa protein. J. Biol. Chem. **273**, 33825–33834.

Hippisley-Cox, J., Coupland, C., Robson, J., Sheikh, A., Brindle, P., (2009). Predicting risk of type 2 diabetes in England and Wales: prospective derivation and validation of QDScore. BMJ **338**, b880.

Houghton, F.J., Bellingham, S.A., Hill, A.F., Bourges, D., Ang, D.K.Y., Gemetzis, T., Gasnereau, I., Gleeson, P.A., (2012). Arl5b is a Golgi-localised small G protein involved in the regulation of retrograde transport. Exp. Cell Res. **318**, 464–477.

Kahn, R.A., Cherfils, J., Elias, M., Lovering, R.C., Munro, S., Schurmann, A., (2006). Nomenclature for the human Arf family of GTP-binding proteins: ARF, ARL, and SAR proteins. J. Cell Biol. **172**, 645–650.

Larkins, C.E., Aviles, G.D.G., East, M.P., Kahn, R.A., Caspary, T., (2011). Arl13b regulates ciliogenesis and the dynamic localization of Shh signaling proteins. Mol. Biol. Cell **22**, 4694–4703.

Lin, C.I., Orlov, I., Ruggiero, A.M., Dykes-Hoberg, M., Lee, A., Jackson, M., Rothstein, J.D., (2001). Modulation of the neuronal glutamate transporter EAAC1 by the interacting protein GTRAP3-18. Nature **410**, 84–88.

Lowe, S.L., Wong, S.H., Hong, W., (1996). The mammalian ARF-like protein 1 (Arl1) is associated with the Golgi complex. J. Cell Sci. **109** (Pt 1), 209–220.

Mahajan, A., Taliun, D., Thurner, M., Robertson, N.R., Torres, J.M., Rayner, N.W., Payne, A.J., Steinthorsdottir, V., Scott, R.A., Grarup, N., et al., (2018). Fine-mapping type 2 diabetes loci to single-variant resolution using high-density imputation and islet-specific epigenome maps. Nat. Genet. **50**, 1505–1513.

Maier, S., Reiterer, V., Ruggiero, A.M., Rothstein, J.D., Thomas, S., Dahm, R., Sitte, H.H., Farhan, H., (2009). GTRAP3-18 serves as a negative regulator of Rab1 in protein transport and neuronal differentiation. J. Cell. Mol. Med. **13**, 114–124.

Marion, V., Stoetzel, C., Schlicht, D., Messaddeq, N., Koch, M., Flori, E., Danse, J.M., Mandel, J.-L., Dollfus, H., (2009). Transient ciliogenesis involving Bardet-Biedl syndrome proteins is a fundamental characteristic of adipogenic differentiation. Proc. Natl. Acad. Sci. U. S. A. **106**, 1820–1825.

Martin, B.R., Cravatt, B.F., (2009). Large-scale profiling of protein palmitoylation in mammalian cells. Nat. Methods **6**, 135–138.

McLaughlin, R.E., Denny, J.B., (1999). Palmitoylation of GAP-43 by the ER-Golgi intermediate compartment and Golgi apparatus. Biochim. Biophys. Acta **1451**, 82–92.

McMahon, H.T., Ushkaryov, Y.A., Edelmann, L., Link, E., Binz, T., Niemann, H., Jahn, R., Südhof, T.C., (1993). Cellubrevin is a ubiquitous tetanus-toxin substrate homologous to a putative synaptic vesicle fusion protein. Nature **364**, 346–349.

Misaki, R., Nakagawa, T., Fukuda, M., Taniguchi, N., Taguchi, T., (2007). Spatial segregation of degradation- and recycling-trafficking pathways in COS-1 cells. Biochem. Biophys. Res. Commun. **360**, 580–585.

Narayan, K.M.V., Boyle, J.P., Thompson, T.J., Gregg, E.W., Williamson, D.F., (2007). Effect of BMI on lifetime risk for diabetes in the U.S. Diabetes Care **30**, 1562–1566.

Nie, Z., Hirsch, D.S., Randazzo, P.A., (2003). Arf and its many interactors. Curr. Opin. Cell Biol. **15**, 396–404.

Panic, B., Whyte, J.R.C., Munro, S., (2003). The ARF-like GTPases Arl1p and Arl3p act in a pathway that interacts with vesicle-tethering factors at the Golgi apparatus. Curr. Biol. CB **13**, 405–410.

Ren, W., Jhala, U.S., Du, K., (2013). Proteomic analysis of protein palmitoylation in adipocytes. Adipocyte **2**, 17–28.

Ren, W., Sun, Y., Du, K., (2015). Glut4 palmitoylation at Cys223 plays a critical role in Glut4 membrane trafficking. Biochem. Biophys. Res. Commun. **460**, 709–714.

Richards, J.B., Waterworth, D., O'Rahilly, S., Hivert, M.-F., Loos, R.J.F., Perry, J.R.B., Tanaka, T., Timpson, N.J., Semple, R.K., Soranzo, N., et al., (2009). A genome-wide association study reveals variants in ARL15 that influence adiponectin levels. PLoS Genet. **5**, e1000768.

Rocha, N., Payne, F., Huang-Doran, I., Sleigh, A., Fawcett, K., Adams, C., Stears, A., Saudek, V., O'Rahilly, S., Barroso, I., et al., (2017). The metabolic syndrome-associated small G protein ARL15 plays a role in adipocyte differentiation and adiponectin secretion. Sci. Rep. **7**, 17593.

Rocks, O., Gerauer, M., Vartak, N., Koch, S., Huang, Z.-P., Pechlivanis, M., Kuhlmann, J., Brunsveld, L., Chandra, A., Ellinger, B., et al., (2010). The palmitoylation machinery is a spatially organizing system for peripheral membrane proteins. Cell **141**, 458–471.

Roy, K., Jerman, S., Jozsef, L., McNamara, T., Onyekaba, G., Sun, Z., Marin, E.P., (2017). Palmitoylation of the ciliary GTPase ARL13b is necessary for its stability and its role in cilia formation. J. Biol. Chem. **292**, 17703–17717.

Scott, R.A., Fall, T., Pasko, D., Barker, A., Sharp, S.J., Arriola, L., Balkau, B., Barricarte, A., Barroso, I., Boeing, H., et al., (2014). Common genetic variants highlight the role of insulin resistance and body fat distribution in type 2 diabetes, independent of obesity. Diabetes **63**, 4378–4387.

Scott, R.A., Lagou, V., Welch, R.P., Wheeler, E., Montasser, M.E., Luan, J., Mägi, R., Strawbridge, R.J., Rehnberg, E., Gustafsson, S., et al., (2012). Large-scale association analyses identify new loci influencing glycemic traits and provide insight into the underlying biological pathways. Nat. Genet. **44**, 991–1005.

Setty, S.R.G., Shin, M.E., Yoshino, A., Marks, M.S., Burd, C.G., (2003). Golgi recruitment of GRIP domain proteins by Arf-like GTPase 1 is regulated by Arf-like GTPase 3. Curr. Biol. CB **13**, 401–404.

Shin, H.-W., Kobayashi, H., Kitamura, M., Waguri, S., Suganuma, T., Uchiyama, Y., Nakayama, K., (2005). Roles of ARFRP1 (ADP-ribosylation factor-related protein 1) in post-Golgi membrane trafficking. J. Cell Sci. **118**, 4039–4048.

Suh, J.M., Gao, X., McKay, J., McKay, R., Salo, Z., Graff, J.M., 2006. Hedgehog signaling plays a conserved role in inhibiting fat formation. Cell Metab. 3, 25–34.

Tang, Q.Q., Lane, M.D., (2012). Adipogenesis: from stem cell to adipocyte. Annu. Rev. Biochem. **81**, 715–736.

Thomsen, S.K., Ceroni, A., van de Bunt, M., Burrows, C., Barrett, A., Scharfmann, R., Ebner, D., McCarthy, M.I., Gloyn, A.L., (2016). Systematic Functional Characterization of Candidate Causal Genes for Type 2 Diabetes Risk Variants. Diabetes **65**, 3805–3811.

Vento, M.T., Zazzu, V., Loffreda, A., Cross, J.R., Downward, J., Stoppelli, M.P., Iaccarino, I., (2010). Praf2 is a novel Bcl-xL/Bcl-2 interacting protein with the ability to modulate survival of cancer cells. PloS One **5**, e15636.

Wei, X., Song, H., Semenkovich, C.F., (2014). Insulin-regulated protein palmitoylation impacts endothelial cell function. Arterioscler. Thromb. Vasc. Biol. **34**, 346–354.

Wu, Y., Yang, M., Fan, J., Peng, Y., Deng, L., Ding, Y., Yang, R., Zhou, J., Miao, D., Fu, Q., (2014). Deficiency of osteoblastic Arl6ip5 impaired osteoblast differentiation and enhanced osteoclastogenesis via disturbance of ER calcium homeostasis and induction of ER stress-mediated apoptosis. Cell Death Dis. **5**, e1464.

Xue, Y., Liu, Z., Cao, J., Ren, J., (2011). Computational Prediction of Post-Translational Modification Sites in Proteins, Systems and Computational Biology - Molecular and Cellular Experimental Systems. IntechOpen.

Yaghootkar, H., Scott, R.A., White, C.C., Zhang, W., Speliotes, E., Munroe, P.B., Ehret, G.B., Bis, J.C., Fox, C.S., Walker, M., et al., (2014). Genetic evidence for a normal-weight "metabolically obese" phenotype linking insulin resistance, hypertension, coronary artery disease, and type 2 diabetes. Diabetes **63**, 4369–4377.

Yu, J., Ka, S.-O., Kwon, K.-B., Lee, S.-M., Park, J.-W., Park, B.-H., (2011). Overexpression of the small GTPase Arl4D suppresses adipogenesis. Int. J. Mol. Med. **28**, 793–798.

Zhao, J., Wang, M., Deng, W., Zhong, D., Jiang, Y., Liao, Y., Chen, B., Zhang, X., (2017). ADP-ribosylation factor-like GTPase 15 enhances insulin-induced AKT phosphorylation in the IR/IRS1/AKT pathway by interacting with ASAP2 and regulating PDPK1 activity. Biochem. Biophys. Res. Commun. **486**, 865–871.

Zhou, C., Cunningham, L., Marcus, A.I., Li, Y., Kahn, R.A., (2006). Arl2 and Arl3 regulate different microtubule-dependent processes. Mol. Biol. Cell **17**, 2476–2487.

Zhou, F., Xue, Y., Yao, X., Xu, Y., (2006). CSS-Palm: palmitoylation site prediction with a clustering and scoring strategy (CSS). Bioinforma. Oxf. Engl. **22**, 894–896.
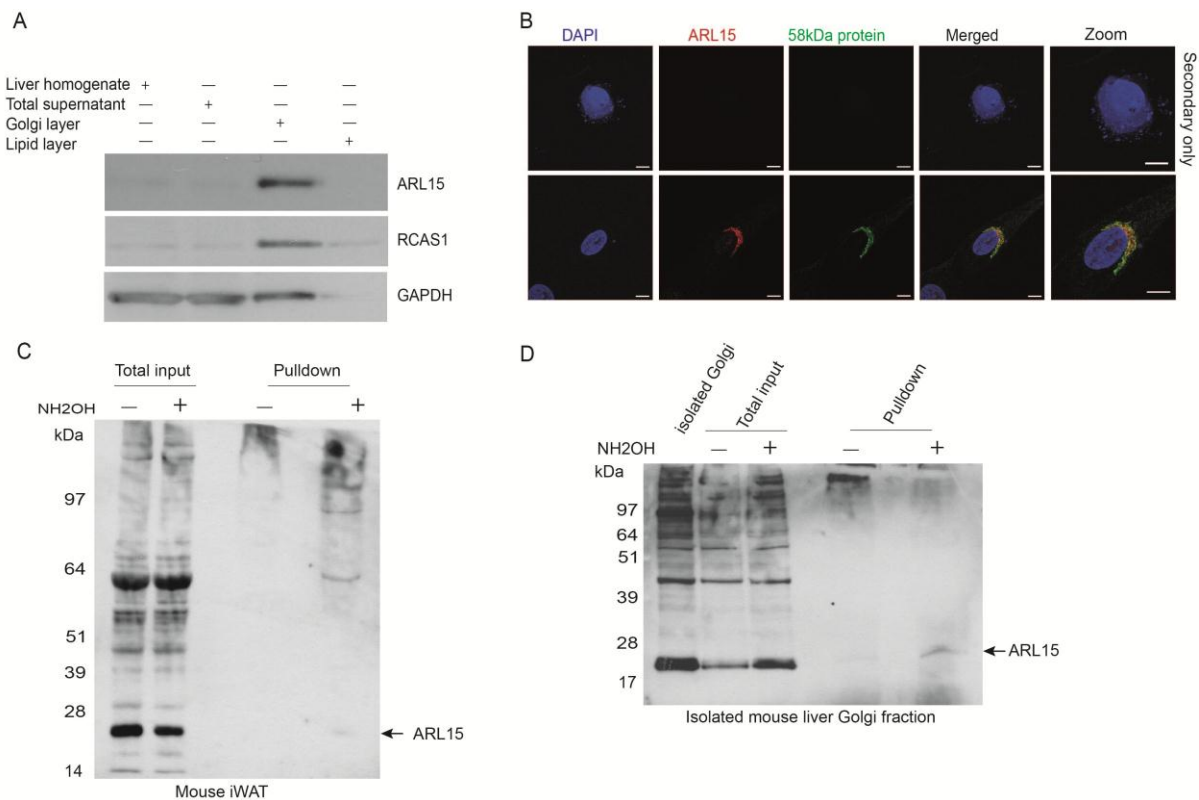
Figures

Figure 1. Endogenous and palmitoylated ARL15 is predominantly localised in Golgi

(**A**) ARL15 is found to be enriched in the Golgi fraction. RCAS1: Golgi marker, GAPDH: loading control; (**B**) Subcellular localisation by immunofluorescence for ARL15. Human white adipocytes co stained with anti-58kDa protein. Secondary antibodies Alexa-488 and Alexa-568 conjugated. Scale bars=10 µm (**C**) Detection of ARL15 palmitoylation in purified Golgi of mouse inguinal white adipose tissue (iWAT) by S-acylated resin-assisted capture (RAC) and immunoblotting with anti-ARL15. Total input and eluted fraction from NaCl-containing control (indicated as "−") and NH$_2$OH-treated samples (indicated as "+") (**D**) Palmitoylated ARL15 is present in purified Golgi of mouse liver as detected by RAC and Western blot.
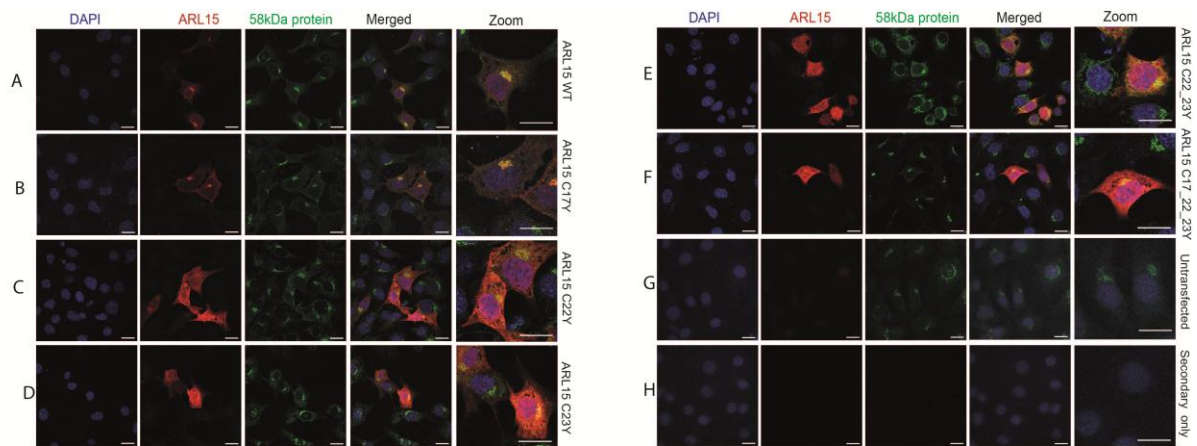
Figure 2. Palmitoylation is required for ARL15 to establish its predominant Golgi localisation

Immunostaining against Myc-tag and 58kDa protein in 3T3-L1 cells overexpressing (**A**) C-terminal Myc-tagged WT ARL15 and palmitoylation-defect mutants, (**B**) ARL15 C17Y, (**C**) ARL15 C22Y, (**D**) ARL15 C23Y, (**E**) ARL15 C22_23Y, (**F**) ARL15 C17_22_23Y, (**G**) untransfected and (**H**) secondary antibody only. Secondary antibodies: Alexa-488 and Alexa-568 conjugated. Scale bars=10 μm
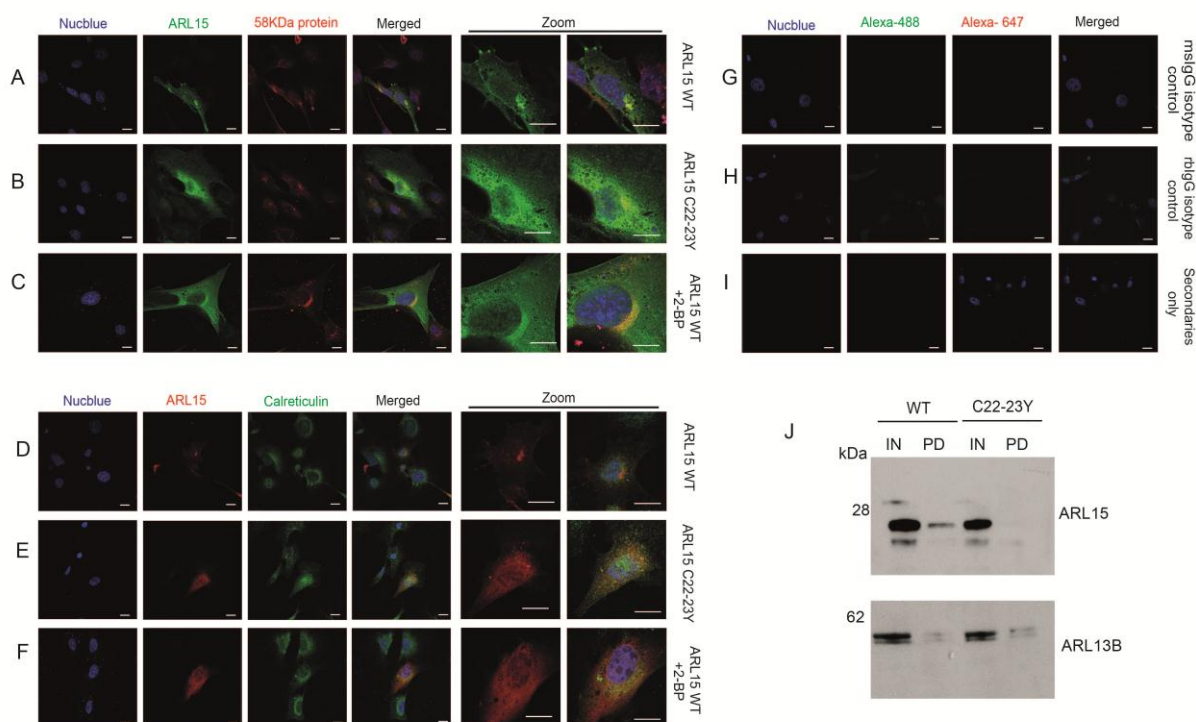
Figure 3. Residues Cys22 and Cys23 are the palmitoylation sites for ARL15 and are essential for the protein's Golgi localisation

Immunostaining against Myc-tag and 58kDa protein in 3T3-L1 cells overexpressing **(A)** C-terminal Myc-tagged WT ARL15, **(B)** palmitoylation-defect mutant ARL15 C22_23Y and **(C)** ARL15 WT treated with 100µM 2-BP inhibitor. Cells were also co-stained with Myc-tag and Calreticulin **(D-F)**. Species specific isotype controls and secondary only stained cells shown in **(G-I)**. Secondary antibodies: Alexa-488 and Alexa-647 conjugated. Scale bar=20 µm **(J)** Representative image of Acyl-RAC assay followed by immunoblotting against ARL15 and ARL13B in lysates of 3T3-L1 cells expressing Myc-tagged WT ARL15 or ARL15 C22_23Y. 3 separate repeats at different passage were performed.

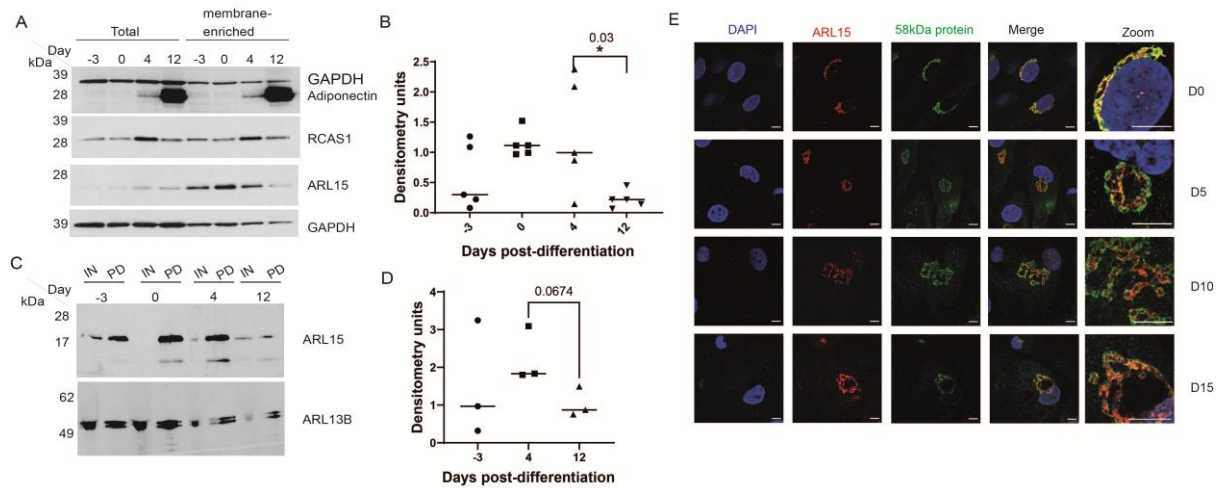IN: input lysates, PD: pull down lysates

Figure 4. ARL15 travels within Golgi from the Cis-side to other parts of Golgi during adipogenesis

(**A**) Western blot showing ARL15, adiponectin and RCAS1 levels in total cell lysate and membrane-enriched fractions in a time course experiment (Days post-differentiation induction). GAPDH and RCAS1are included for comparison.

(**B**) Level of ARL15 at D12 post-differentiation induction is significantly reduced comparing to D4, when differentiation was induced. ARL15 band intensity is relative to GAPDH. Data are presented as mean±s.e.m and analysed by using one-way ANOVA. n=5 replica experiments; * P<0.05 (**C**) ARL15 palmitoylation over 12 days of differentiation in 3T3-L1 cells as detected by S-acylated resin-assisted capture followed by immunoblotting with anti-ARL15 and anti-ARL13B. (**D**) There is a trend towards reduction in ARL15 palmitoylation 12 days post differentiation. Densitometry is relative to input. Data are presented as mean±s.e.m, analysed by t-test between day 4 and day12, n=3 repeats with the same cell line. IN= input fraction, PD= pull-down fraction (**E**) Representative confocal images of hWAT cells co-stained with anti-ARL15 and anti-58kD protein (Cis Golgi marker) Secondary antibodies: Alexa-488 and Alexa-647 conjugated. Scale bar=10 µm; Scale bars for zoom in image are 5 µm
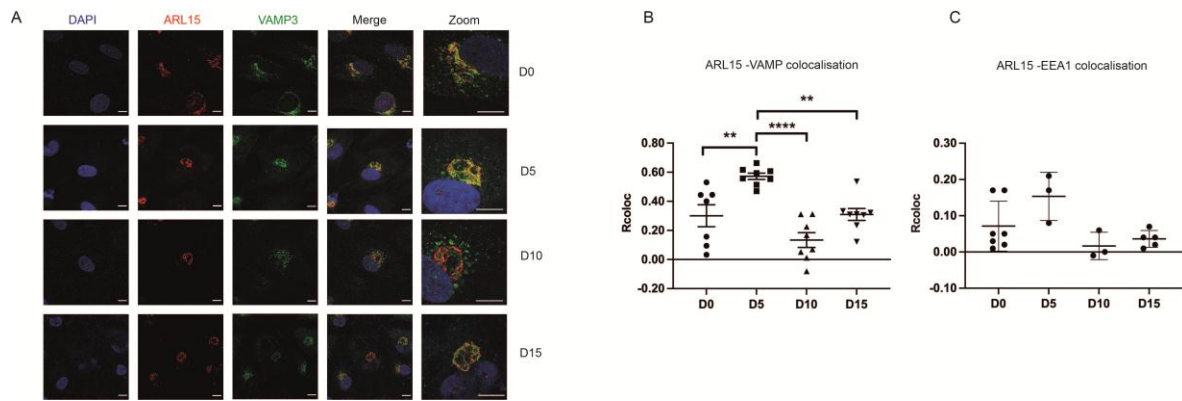
Figure 5. ARL15 partially colocalises with VAMP3 at early stage of adipogenesis

(**A**) Representative confocal images of hWAT cells co-stained with anti-ARL15 and anti-VAMP3 protein (recycling endosome localised protein) Secondary antibodies: Alexa-488 and Alexa-647 conjugated. Scale bar=10 µm; Scale bars for zoom in image are 5 µm. Colocalisation analysis (Pearson correlation coefficient) during differentiation for ARL15 and VAMP3 (**B**) and ARL15 and EEA1 (**C**) proteins Colocalisation coefficients are presented as mean±s.e.m and analysed by using one-way ANOVA. ** P<0.01, **** P<0.0001. Scale bar=10 µm
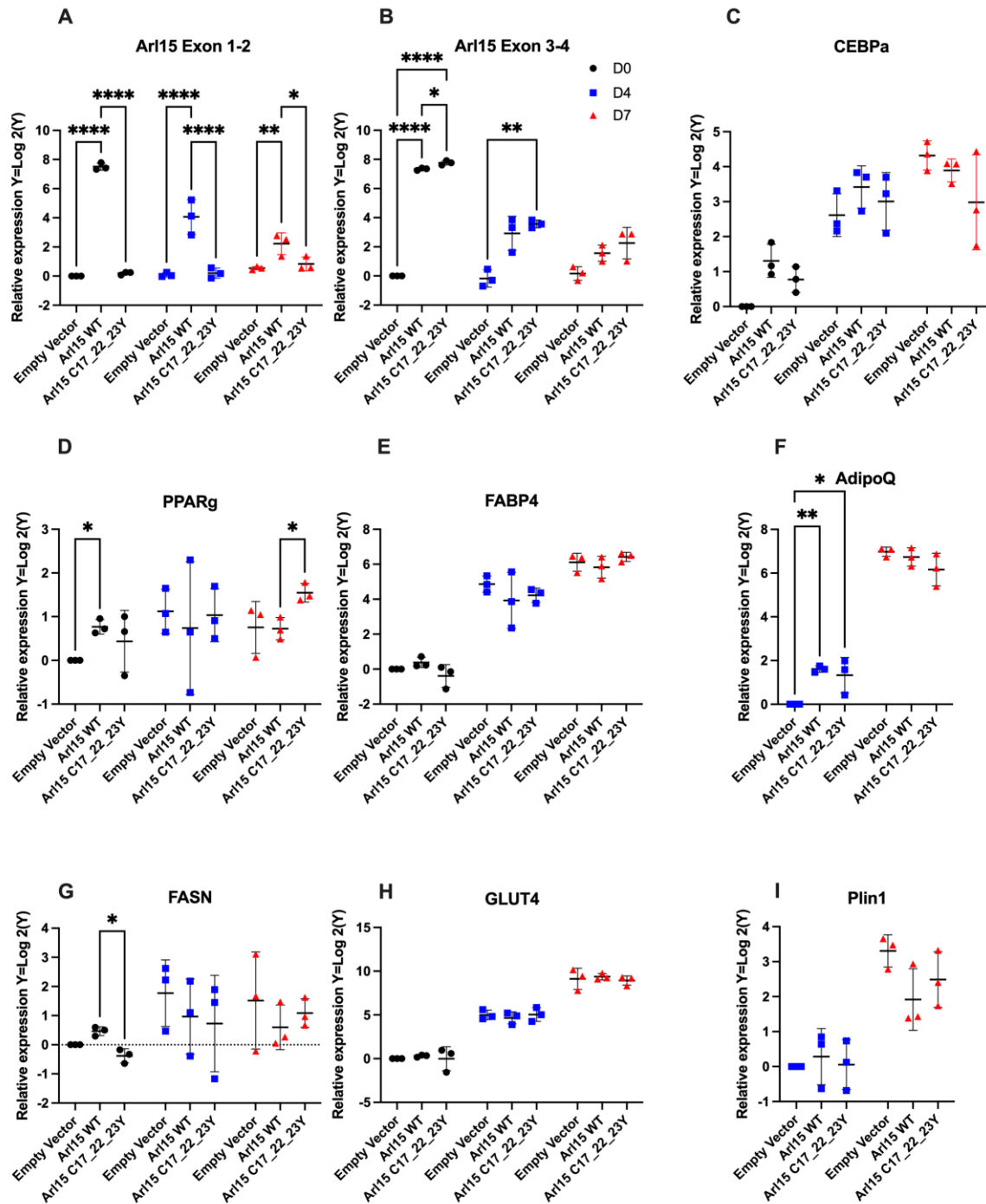
Figure 6. *Arl15* overexpression reduces levels of late-stage adipogenesis-related genes

(**A-I**) q-RT-PCR for relative expression of *Arl15*, adipogenic and lipogenic genes in cells over-expressing WT and mutant ARL15 17_22_23Y in 3T3L1 cells at day 0, 4 and 7 of differentiation. Data are normalised to empty vector at day 0, with the exception of *AdipoQ* and *Plin1* that are expressed at very low levels at that time point and are consequently normalised to day 4. Data are Log 2 transformed with

mean±s.d.from triplicates and analysed using two-way ANOVA with comparisons between the three vectors at each timepoint using Tukey's multiple comparison test. * P<0.05; ** P < 0.01; ****P< 0.0001
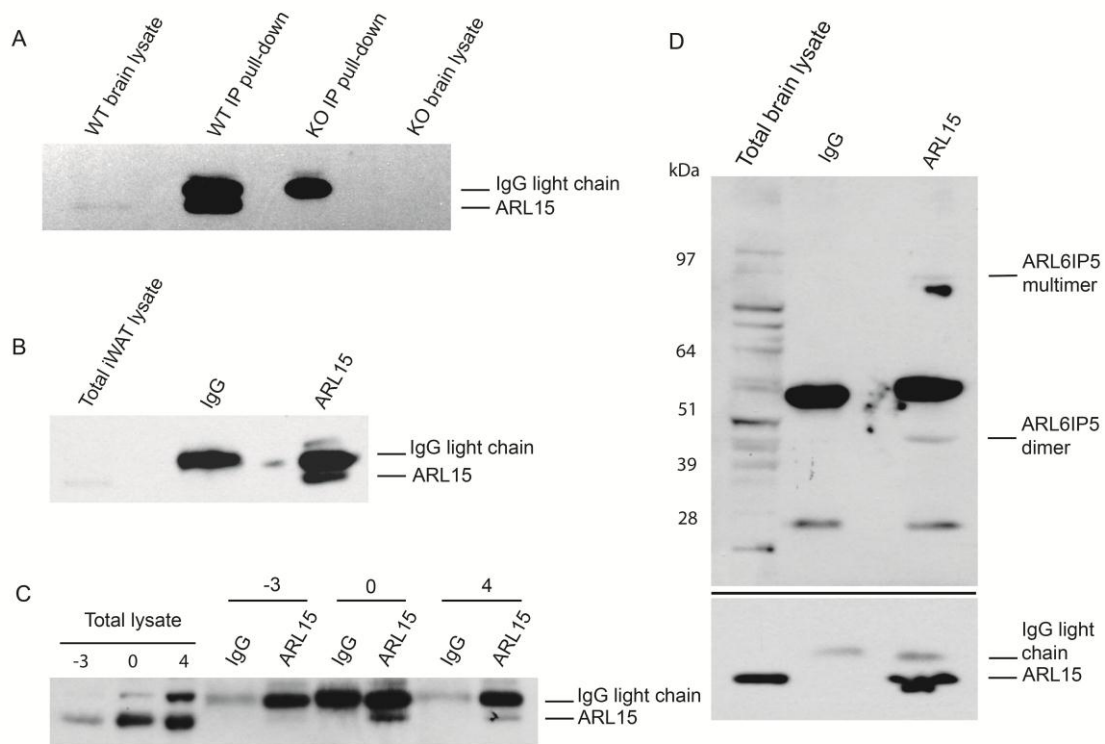
Figure 7. Protein-protein interactions between ARL15 and ARL6IP5

(**A**) Mouse brain lysates and those from homozygous *Arl15* knockout mouse were immunoprecipitated with an ARL15 antibody and probed for the presence of ARL15 by western blot analysis. Total lysates were also probed for the presence of the endogenous ARL15. (**B**) The mouse iWAT lysates were immunoprecipitated with an ARL15 antibody and probed for the presence of ARL15 by western blot analysis. As a control, the lysates were also incubated with a rabbit IgG antibody. Total lysates were probed for the presence of the endogenous ARL15. (**C**) The 3T3-L1lysates were immunoprecipitated with an ARL15 antibody and probed for the presence of ARL15 by western blot analysis. As a control, the lysates were also incubated with a rabbit IgG antibody. Total lysates were probed for the presence of the endogenous ARL15. (**D**) Mouse brain lysate was immunoprecipitated with an ARL15 antibody and probed for the presence of ARL15 (or ARL6IP5) by western blot analysis. As a control, the lysates were also incubated with a rabbit IgG antibody. Total lysates were probed for the presence of the endogenous ARL15 and ARL6IP5.

Tables

Table 1. Potential ARL15 Co-IP interacting partners identified by mass spectrometry and appearing more than once in different experiments

Sample	Brain	iWAT	3T3-L1 (replicate 1)	3T3-L1 (replicate 2)	3T3-L1 (replicate 3)
	ARL15	ARL15	ARL15	ARL15	ARL15
	ARL6IP5	ARL6IP5	ARL6IP5	ARL6IP5	
		FAM98B	FAM98B	FAM98B	
		COG6	COG6		
		MTMR2	MTMR2		
			MTMR12		MTMR12
		MYBBP1A		MYBBP1A	MYBBP1A
		DNPEP		DNPEP	DNPEP
				PRSS1	PRSS1
				MICAL2	MICAL2
				PLAC8	PLAC8
		MCCC2		MCCC2	MCCC2
		AP2A1&2			AP2A1&2
		HEXIM2	HEXIM2		HEXIM2

Brain: whole mouse brain. iWAT: mouse subcutaneous inguinal white adipose tissue. 3T3L1: mouse pre-adipocyte cell line. Knockout mouse brain tissue was used as a negative control in the whole brain IP. For iWAT adipose tissue and 3T3L1 adipose cell line IP experiments IgG was used as a negative control. Only potential interacting proteins found in the ARL15 but not the control immunoprecipitations are listed.
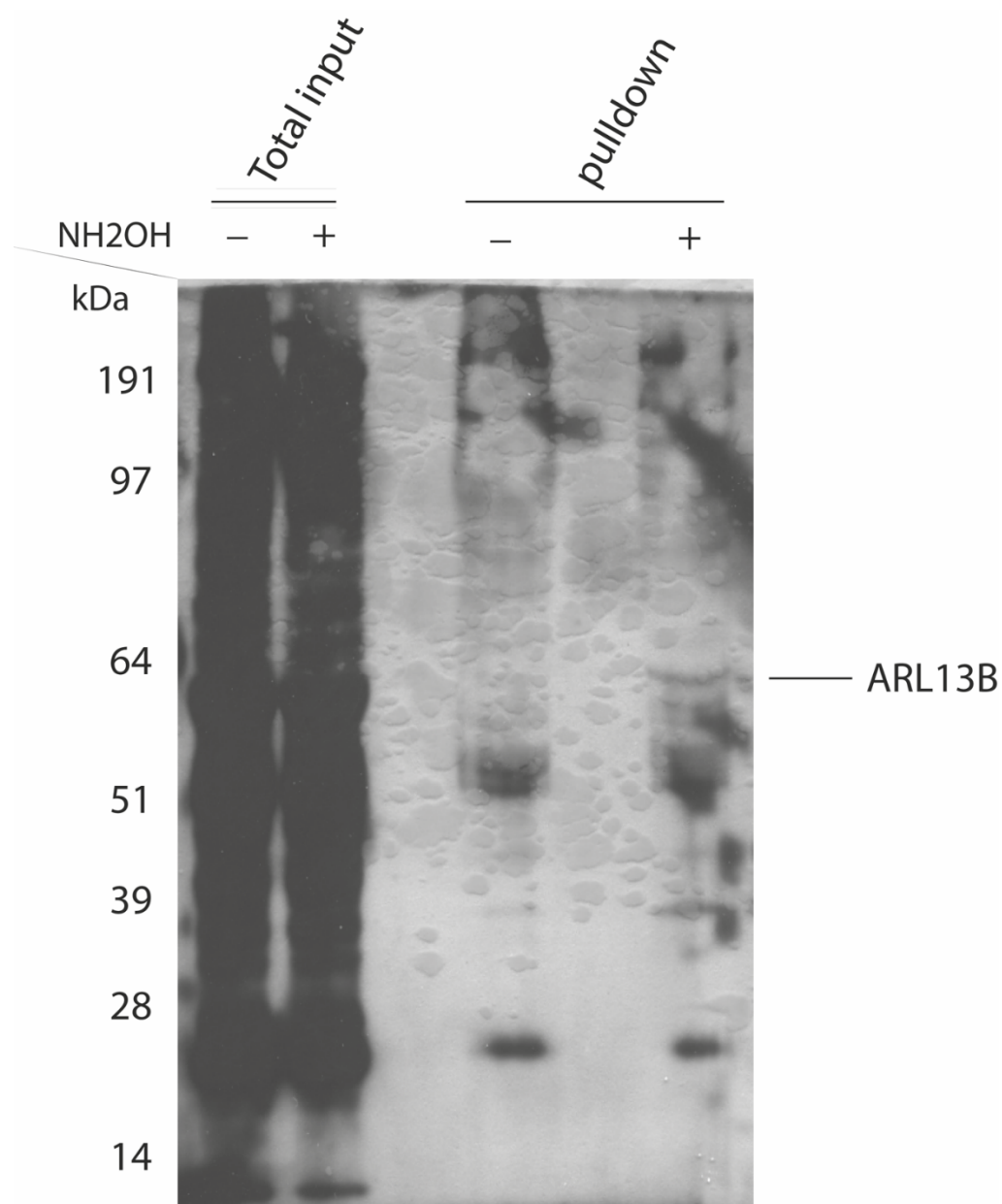
Fig. S1. ARL13B, a known palmitoylated protein is detectable in mouse inguinal white adipose tissue (iWAT) by RAC.

The detection of palmitoylation of ARL13b from mouse iWAT was carried out by acyl-RAC and western blot. Samples were treated with a final concentration of 0.2 M NH$_2$OH or 0.2 M NaCl as a control and then palmitoylated proteins were enriched using prewashed thiopropyl Sepharose beads. Enriched samples were eluted using binding buffer containing 50 mM DTT at room temperature for 20 minutes. Total input and eluted fraction from NaCl-containing control (indicated as "−") and NH$_2$OH-treated samples (indicated as "+") were separated by SDS-PAGE followed by western blotting with a primary antibody to ARL13B.
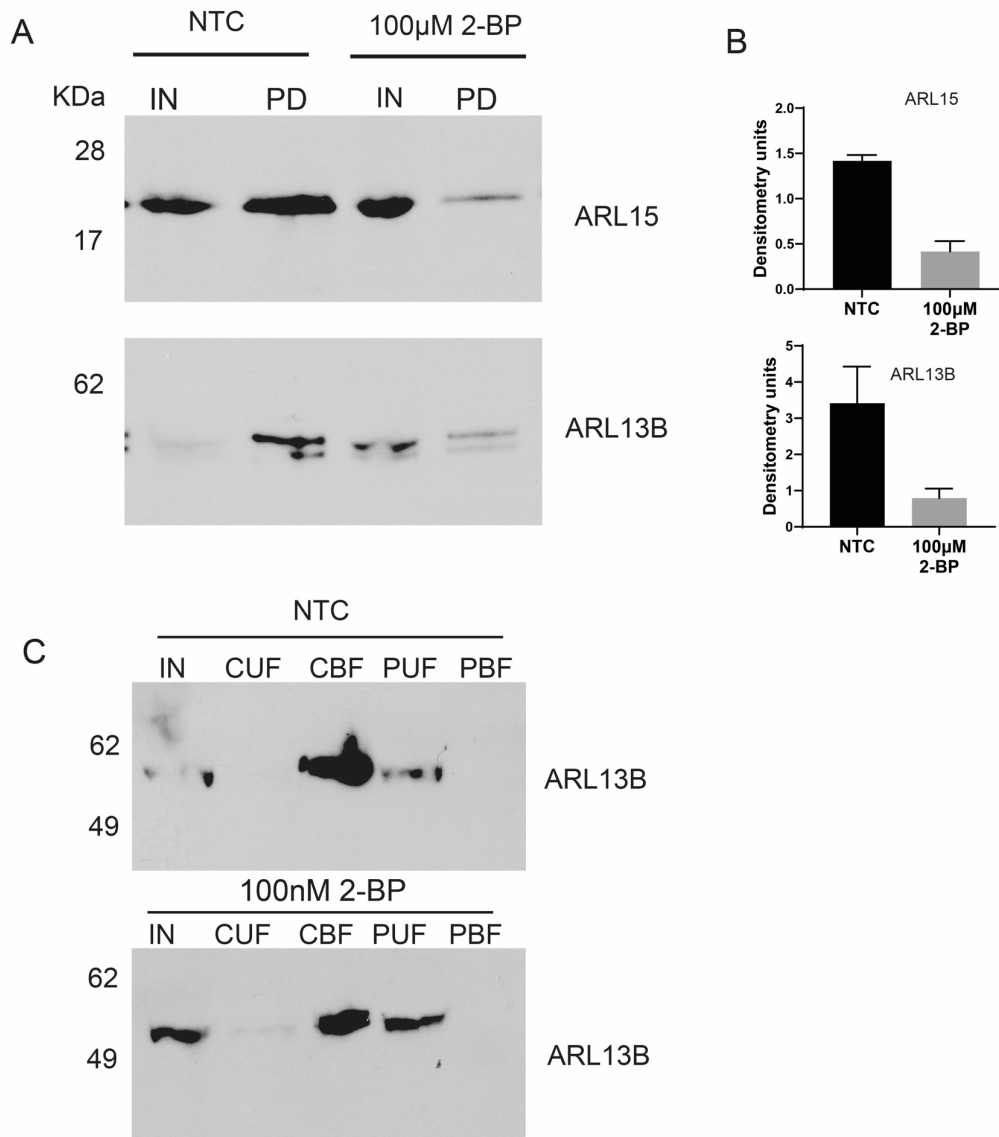
Fig. S2. 2-bromopalmitate (2-BP), a known blocker of palmitate incorporation inhibits ARL15 and ARL13B palmitoylation.

(A)Treatment with 100μM 2-BP overnight resulted in significantly reduced palmitoylation of ARL15 and ARL13B in 3T3-L1 cells compared to non-treated control cells (NTC) as detected by S-acylated resin-assisted capture (RAC) and western blot. (B) Densitometry for ARL15 and ARL13B. Densitometry is relative to input, data presented as mean±s.e.m, n=2. (C) Representative image of the S-acylated RAC generated fractions showing enrichment of the cleaved bound fraction, complete cysteine blocking and specific binding of protein in the resin as indicated by the absence of the preserved bound fraction. This example was also treated with 100nM 2-BP overnight, although this does not significantly inhibit palmitoylation. NTC: non-treated control lysates, PD: pull down lysates, IN: input fraction, CUF: cleaved unbound fraction, CBF: cleaved bound fraction/pull-down, PUF: preserved unbound fraction, PBF: preserved bound fraction.
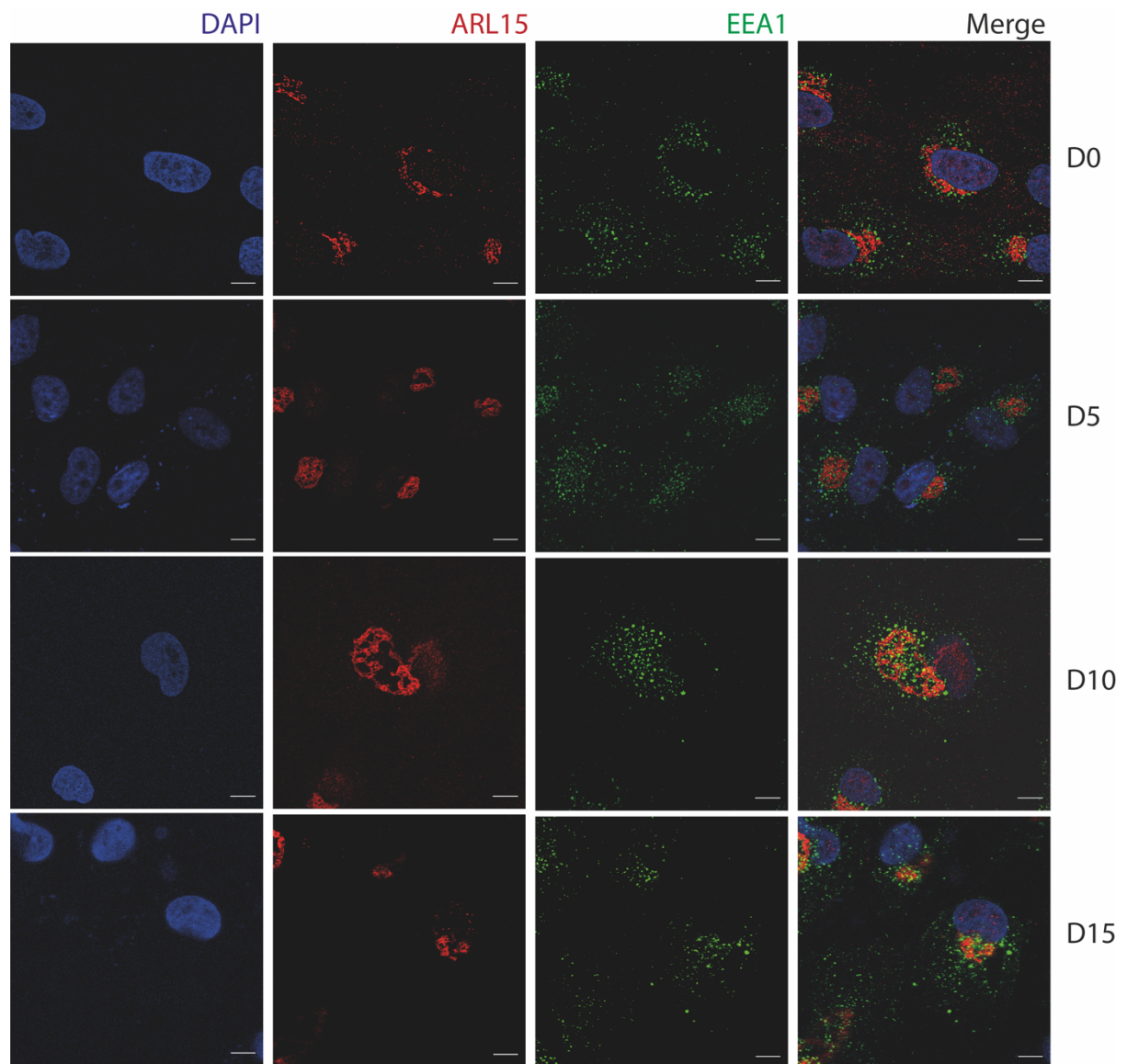
Fig. S3. ARL15 is not localised in early endosome.

Representative confocal images of hWAT cells were co-stained with anti-ARL15 and anti-EEA-1 (early endosome marker) antibodies followed by incubating with secondary antibody conjugated with Alexa-568 (red) and Alexa-488 (green). Scale bar=10 μm
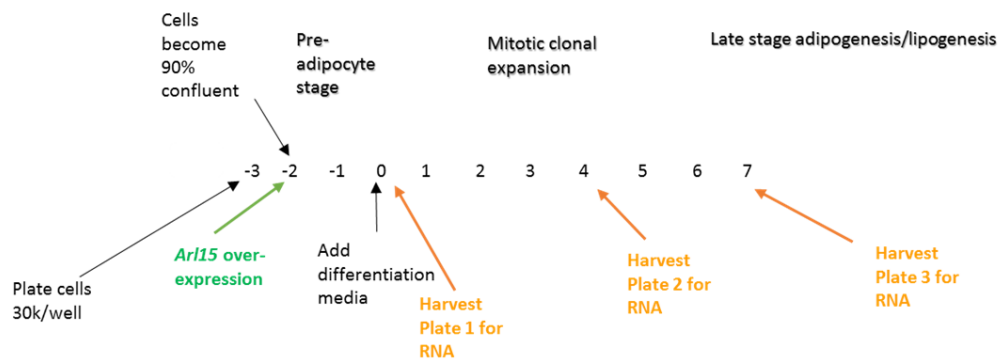
Fig. S4. Experimental plan for 3T3-L1 cell differentiation and Arl15 overexpression (WT and mutant Arl15 17_22_23Y) in 3T3-L1 adipocytes.

3T3-L1 preadipocytes were plated at 30k/well 3 days prior to adipogenesis induction (D-3). Cells were lipofectamine-transfected with WT or mutant Arl15 (C17_22_23Y) on D-2. 48 hours post-transfection, differentiation medium was added (D0). Cells were cultured until harvest for analysis at D0, D4 and D7 post-differentiation induction.

Table S1. ARL15 has three palmitoylation sites at its N-terminal (Cys17, Cys22 and Cys23) predicted by the clustering and scoring strategy algorithm CSS-Palm 4.0. The score calculated by algorithm CSS-Palm corresponds to the confidence of the palmitoylation of the tested peptide; the cut-off score corresponds to the sensitivity and specificity of CSS-Palm (Zhou et al., 2006). A high threshold pre-set by the developer was selected for palmitoylation sites prediction.

ID	Position	Peptide	Score	Cutoff
sp|Q8BGR6|ARL15_MOUSE ADP-ribosylation factor-like protein 15 OS=Mus musculus OX=10090 GN=Arl15 PE=1 SV=1	17	FLYMDYLCFRALCCK	22.841	4.222
sp|Q8BGR6|ARL15_MOUSE ADP-ribosylation factor-like protein 15 OS=Mus musculus OX=10090 GN=Arl15 PE=1 SV=1	22	YLCFRALCCKGPPPA	7	3.419
sp|Q8BGR6|ARL15_MOUSE ADP-ribosylation factor-like protein 15 OS=Mus musculus OX=10090 GN=Arl15 PE=1 SV=1	23	LCFRALCCKGPPPAR	15.222	4.222

References

ZHOU, F., XUE, Y., YAO, X. & XU, Y. 2006. CSS-Palm: palmitoylation site prediction with a clustering and scoring strategy (CSS). *Bioinformatics,* 22**,** 894-896.